Imaging of 32-nm 1:1 lines and spaces using 193-nm immersion interference lithography with second-generation immersion fluids to achieve a numerical aperture of 1.5 and a k_1 of 0.25

Roger H. French
DuPont Company
Central Research
Wilmington, Delaware 19880-0356

Harry Sewell
ASML
Wilton, Connecticut 06877

Min K. Yang
Sheng Peng
DuPont Company
Central Research
Wilmington, Delaware 19880-0356

Diane McCafferty
ASML
Wilton, Connecticut 06877

Weiming Qiu
Robert C. Wheland
Michael F. Lemon
DuPont Company
Central Research
Wilmington, Delaware 19880-0356

Louis Markoya
ASML
Wilton, Connecticut 06877

Michael K. Crawford
DuPont Company
Central Research
Wilmington, Delaware 19880-0356

Abstract. Water-based immersion lithography using ArF illumination is able to provide optical solutions as far as the 45-nm node, but is not able to achieve the 38- or 32-nm nodes as currently defined. Achieving these lithographic nodes will require new, higher refractive index fluids to replace the water used in first-generation immersion systems. We have developed a number of such second-generation high-index fluids for immersion lithography at 193 nm. These highly transparent fluids have 193-nm indices up to 1.664. To understand the behavior and performance of different fluid classes, we use spectral index measurements to characterize the index dispersion, coupled with Urbach absorption edge analysis and Lorentz Oscillator modeling. Interference imaging printers have long been available, and they now have a new use: a rapid, cost-effective way to develop immersion lithography, particularly at extremely high resolutions. Although interference printers will never replace classical lens-based lithography systems for semiconductor device production, they do offer a way to develop resist and fluid technology at a relatively low cost. Their simple image-forming format offers easy access to the basic physics of advanced imaging. Issues such as polarization of the image-forming light rays, fluid/resist interaction during exposure, topcoat film performance, and resist line edge roughness (LER) at extremely high resolutions, can all be readily studied. 32-nm 1:1 line/space (L/S) imaging is demonstrated using two of the second-generation fluids. These resolutions are well beyond current lens-based system capabilities. Results on the performance of various resists and topcoats are also reported for 32-nm L/S features. [DOI: 10.1117/1.2039953]

Subject terms: 32-nm node; 38-nm node; high-*n* immersion fluids; ArF immersion lithography; 193-nm immersion lithography.

Paper 05023SSR received Mar. 29, 2005; revised manuscript received May 24, 2005; accepted for publication Jun. 7, 2005; published online Sep. 2, 2005.

1 Introduction

Optical lithography has been the semiconductor industry's major imaging technique for the past 30 years, and resolution requirements have driven system development. Figure 1 shows the 2004 updated[1] ITRS lithography requirements for both production and leading-edge devices. Optics developments allow current equipment technologies to be pushed as far as the 65-nm node by increasing numerical apertures and decreasing the illumination wavelength to 193-nm (ArF). In addition, lithographic techniques such as off-axis illumination allow processing at k factors as low as 0.30. Introducing water-based immersion lithography in ArF laser-illuminated step-and-scan systems supports the achievement of the 45-nm node.

1.1 *Immersion Lithography with Water (First-Generation Fluid)*

Immersion lithography is being established as a production technology using converted conventional systems such as

1537-1646/2005/$22.00

Fig. 1 Half-pitch linewidth nodes from the 2004 updated ITRS lithographic roadmap.

AT1150i and AT1250i. Initial results (Fig. 2) demonstrate a significant improvement in depth of focus for immersion exposure compared with dry exposure, and they confirm notable improvements in process latitude.

These AT1150i and 1250i systems allow the development of resist systems that are compatible with water as the immersion fluid. The full production introduction of immersion lithography will be on systems such as AT1400i with a numerical aperture of 0.93.

There do not appear to be any show-stoppers to achieving the 45-nm node using immersion lithography. Calculations indicate that a numerical aperture of approximately 1.3 will be required to operate at a k factor of 0.30. Lens design engineers indicate that existing designs meet this requirement, but cost is a concern. It is expected that the 45-nm node will be achieved on the schedule indicated by Fig. 1, with leading edge immersion production in place by 2007.

1.2 *Pushing the Limits of Optical Lithography*

The 38- and 32-nm nodes will be required for leading-edge development work in 2008 and 2009, respectively, representing the next major challenge for optical lithography development. We report early development work designed to define the key requirements for successful immersion lithography at the 32-nm node, and clarify some of the technical issues associated with achieving the 32-nm lithographic node.

The roadmap shown in Fig. 1 indicates that to achieve the 32-nm node with immersion lithography, the optical system numerical aperture will have to be increased to 1.8 for operation with a processing k factor of 0.30. If more aggressive k factors can be used, the target numerical aperture can be lower.

2 Hyper-NA Imaging for the 32-nm Node

2.1 *Imaging with the Interferometric Test Rig*

Two interferometric test rigs for immersion interference lithography are now being used for 45-nm node process development to facilitate the testing of topcoats, fluids, and resists. The version 1 prototype test rig is configured with the resist facing downward; Fig. 3 shows the optical path from the side and under the top plate. Fluid is contained in a well in the test rig and is in contact with the resist surface on the wafer. The test rig is configured with a simple grating beamsplitter to divide a laser beam into three beams: one zero order and two first orders. The zero-order beam is blocked, and the two first-order beams are reflected from mirror surfaces, through a quartz block, and into the fluid well, to recombine and form interference fringes. This is a basic Talbot interferometer. The test rig is configured so that the fringe pattern forms in the fluid at the resist/fluid interface and exposes a line/space pattern in the resist. The fringe spacing (L/S resolution) is controlled by the mirror surface positions. Excellent L/S patterns can be printed and studied. Film stack exposures on an interference test rig allow a number of experiments to be run, and the viability and compatibility of fluids, topcoats, and resists can be assessed under a variety of imaging conditions. Test rigs also allow the testing of new immersion fluids in showerhead configurations on resist-coated wafers.

The version 2 test rig has the resist-coated wafer facing upward and can be used in a two-beam configuration (Fig.

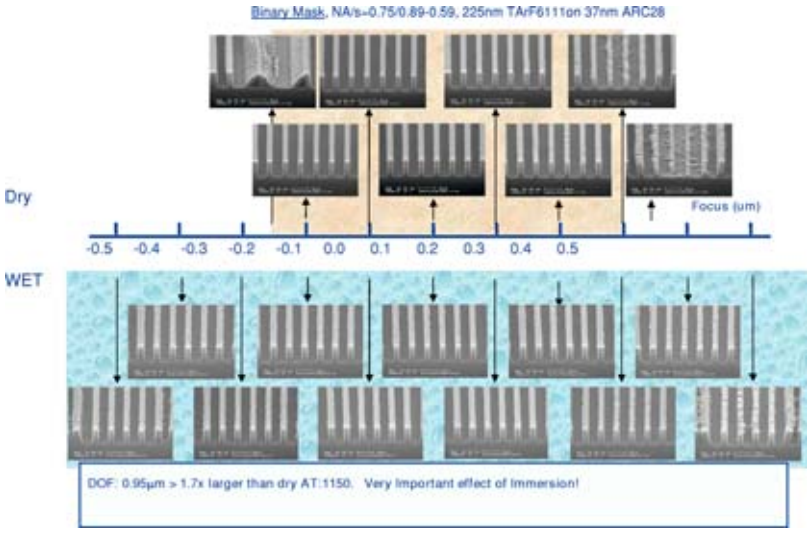

Fig. 2 Comparison of the wet and dry depth of focus for 90-nm dense lines, scanned on a Twinscan AT:1150i. AT1150i data were supplied from the ASML-Veldhoven wafer processing group.

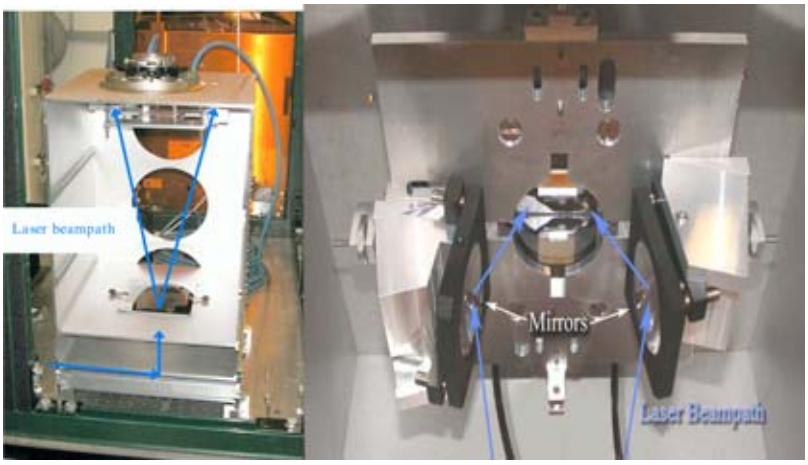

Fig. 3 Version 1 interference test rig showing the optical path.

4) to print L/S patterns or in a four-beam configuration (Fig. 5) to print contact holes. A beamsplitter and reflecting surface configuration is used similar to the version 1 test rig (Talbot interferometer), but the interferometer resolution is varied by interchanging an optics module, rather than by moving mirrors.

Using an interference immersion test rig allows key hyper-NA imaging factors, including polarization effects, to be explored.

2.2 *Polarization in Hyper-NA Imaging*

Simulations of 32-nm L/S printing run on a Solid-C v6.4 simulation program indicate that polarization is a key parameter in image formation and must be set to transverse electrical (TE) mode for adequate image contrast. Figure 6 indicates image contrast for TE and transverse magnetic (TM) mode illumination polarization in addition to image contrast for unpolarized light.

For 32-nm L/S printing, the image-forming beams are angled at approximately 70 deg. to the normal vector in the resist. The two imaging beams are almost orthogonal, and for the beams' TM components, this precludes interference and, therefore, imaging. Only the TE polarization beam component gives an acceptable image. Normalized image log slope (NILS) is simulated using Prolith V9.0 for 45-, 38-, and 32-nm L/S. Figure 7 indicates that image NILS is maximized for s polarization (TE). For p polarization (TM), image-inversion effects are evident on the NILS plot. Polarized light in lithographic imaging systems has been used for many years (ASML/SVGL Micrascan Series Step and Scan Systems). Issues associated with polarized light are

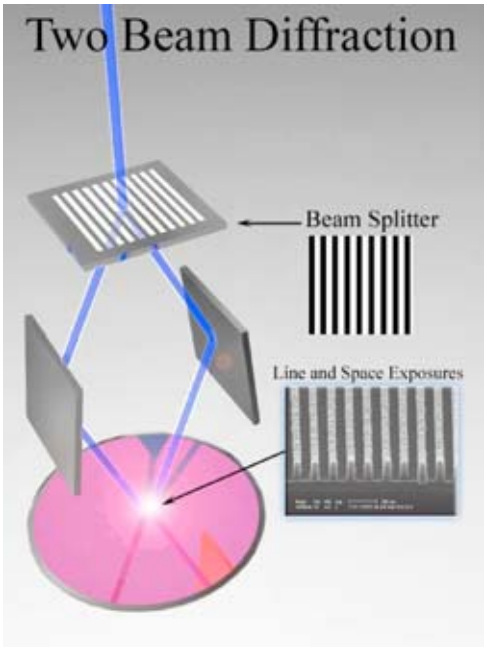

Fig. 4 Two-beam interferometric imager. Sin(θ) and, hence, resolution is set by adjusting the positions and angles of the mirrors.

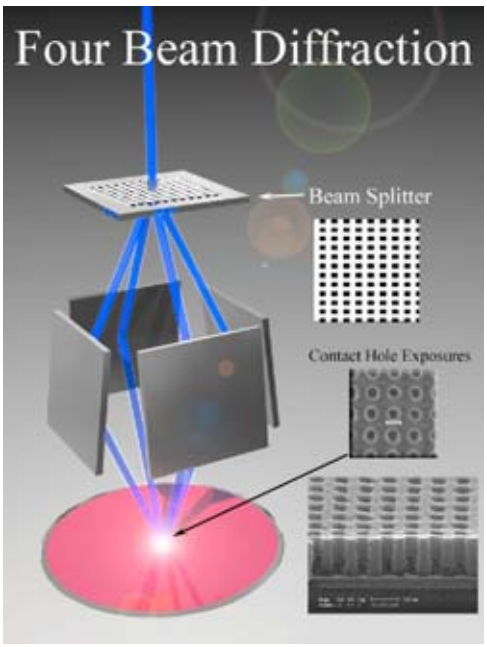

Fig. 5 Four-beam interferometric imager.

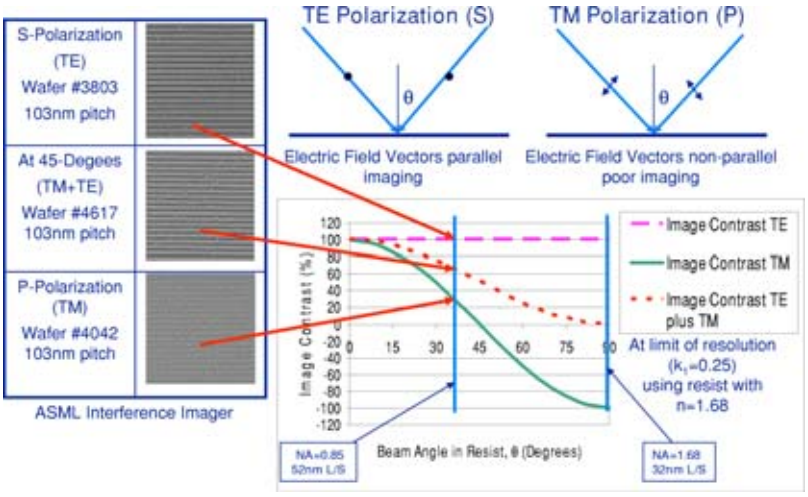

Fig. 6 Image contrast against imaging beam angle for TE and TM polarizations.

well known[2–5] and can be readily controlled. The use of improved, low birefringent glass in lenses, illuminators, and mask blanks is quite usual.

Imaging tests in resist on the immersion test rig have been conducted using TE polarized light to give the maximum image contrast for 32-nm 1:1 L/S patterns.

2.3 *Resist/Immersion Fluid Film Stack for Second-Generation Immersion Lithography*

2.3.1 *Optical requirements*

To assess the implications of this hyper-NA requirement, we must look closely at the resist/fluid film stack (Fig. 8). For light to enter the resist and form the image, it must pass from the lens to the fluid and then to the resist topcoat, and finally, into the resist itself. Snell's law must be obeyed at each interface, and for planar interfaces, the numerical aperture must be maintained.

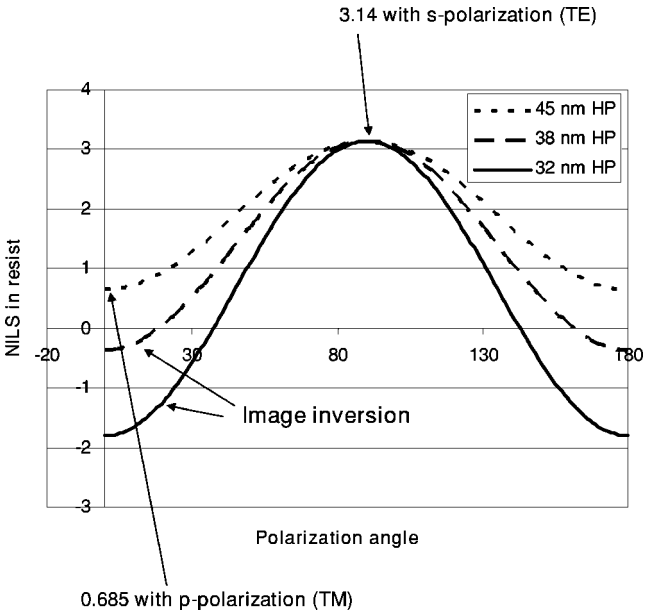

Fig. 7 NILS plot against polarization angle.

$$NA = n_{glass}\sin(\theta_{glass}) = n_{fluid}\sin(\theta_{fluid}) = n_{topcoat}\sin(\theta_{topcoat}) = \ldots$$

Clearly, $\sin(\theta)$ must be less than 1, so the minimum refractive index of the layers in the stack becomes the maximum NA that the film can support. Typical refractive indices for stack materials are: water, 1.44; resist, 1.69; topcoat, 1.65; and quartz glass, 1.56. It is clear that a water immersion fluid with a refractive index of 1.44 will prevent NAs greater than 1.44 from being achieved. Figure 9 plots the resolution against the film stack's minimum refractive index for a range of k factors.

Note that the calculation includes 0.90 as the practical optics limit for $\sin(\theta)$. This requires that the immersion fluid's refractive index be at least 10% higher than the theoretical minimum value. It is also assumed that all other refractive indices in the stack are higher than the fluid's refractive index. There is a relationship between the numerical aperture and the k factor at which the process must operate to give 32-nm node imagery: for an NA of 1.64, the k factor would be 0.27; for an NA of 1.8, the k-factor would be 0.30. The NA is limited by the minimum refractive index in the film stack. Table 1 summarizes the tar-

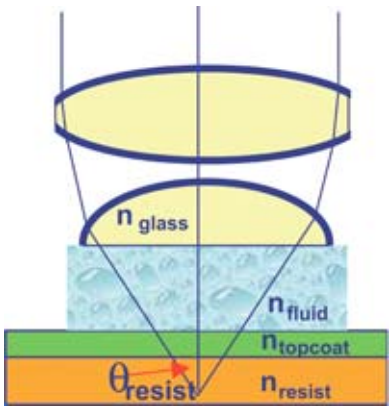

Fig. 8 Immersion lithography film stack.

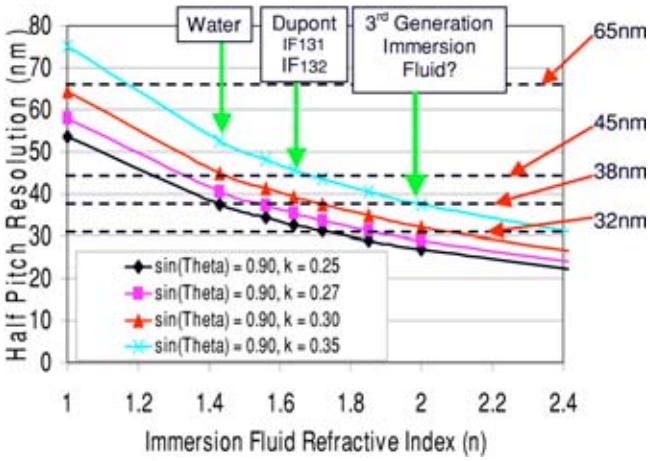

Fig. 9 Half-pitch resolution plotted against immersion fluid refractive index.

geted immersion fluid properties for the 38- and the 32-nm nodes. Not only must the fluid's refractive index be high, but its absorbance at 193 nm also needs to be low—ideally, comparable to that of water. Table 1 also indicates the required immersion fluid properties for the case of a planar final lens surface and for the case of a concave lens surface. For the final lens surface to be planar, high refractive index lens glass must be available.[6]

2.3.2 *Physical property requirements*

The fluid must also be compatible (and preferably completely noninteracting) with resists and topcoats. The fluid's surface-wetting and surface-tension properties on resist and topcoat films are important for immersion system showerhead design and for containing and controlling the fluid.

In addition to the fluid's refractive index requirement, there are two further optical property requirements that are dependent on the final lens element design: absorbance and the temperature coefficient of refractive index. As summarized in Table 1, for a flat final surface, the fluid's optical absorbance should be $<0.15/\mathrm{cm}$. If the final surface is curved, a more stringent absorbance requirement of $<0.03/\mathrm{cm}$ is needed. In addition, the index change with temperature (dn/dT) must be less than 250 ppm/K for a flat final surface, or 50 ppm/K for a curved final surface.

The temperature coefficients of the refractive index and viscosity must be within the design limits of the showerhead and wafer-scan velocity. Finally, the viscosity and surface tension must permit good fluid handling for fast scanning, and the additional cost of ownership must be reasonable.

Fluid-wetting properties can be examined. Table 2 shows fluid contact angle results for the DuPont IF132 immersion fluid compared to water for a number of materials. The data for water imply that the target contact angle value of the high-*n* immersion fluid with resist or topcoat is 75 deg. Fluid performance under showerheads is being tested, and the fluid fill and retrieval is being monitored. The transport of fluid volumes over the wafer/resist surface can be tracked. Figure 10 shows a showerhead compatibility test.

3 Optics of Immersion Fluids

3.1 *VUV Spectroscopy*

In this work, the refractive index was measured by a prism minimum deviation technique using both a J.A. Woollam Company VUV-VASE® and a DUV-VASE spectroscopic ellipsometer system capable of measuring over the spectral ranges 140 to 1700 nm and 187 to 1100 nm, respectively. The optical absorbance was measured by using a relative

Table 1 Properties of immersion fluids for 38- and 32-nm lithography.

	Flat last lens		Concave last lens	
Half-pitch	⩽38 nm	⩽32 nm	<38 nm	<32 nm
Fluid refractive index (*n*)	>1.65	>1.9	>1.65	>1.9
Fluid absorption	<0.15/cm		<0.03/cm	
Fluid dn/dT	<250 ppm/K		<50 ppm/K	
Differential cost of ownership	~1 to 2 $/layer			
Rheology	Comparable to water			
Viscosity	<0.003 Pas			
Surface tension	Similar to water			
Lifetime	Minimal photochemical effects			
Imaging	No degradation impact on imaging from interactions with resist/TC			

Other boundary conditions:
- in case of flat lens element high-*n* glass (>1.65 or >1.9) is needed
- for 32-nm resolution high-*n* resist (>1.9) is needed

Table 2 Immersion fluid contact angles measured on resist and showerhead materials.

		IF132		Deionized water	
		Initial	1 min.	Initial	1 min.
Quartz		15.9	14.4	45.3	37.5
Resist	PAR-817 (70 nm)	22.3	22.0	77.6	75.0
Silicon	(native oxide)	15.9	13.9	4.4	2.7
Stainless steel		7.0	5.0	76.6	61.2
Teflon 1	From holder	54.7	54.3	112.0	109.3
Teflon 2	From cassette	50.0	49.3	78.5	73.9
Topcoat 1	TCX-007 (30 nm)	52.2	53.1	90.6	91.1
Topcoat 2	TSP-3A (38 nm)	66.0	66.4	120.0	118.9

transmission measurement. Optical parameters of various immersion fluids studied are presented in Table 3.

3.1.1 *Index of refraction measurements*

The spectral refractive index is measured[7,8] by using a liquid-filled prism cell mounted on the sample stage. The ellipsometer then determines the minimum deviation angle for light transmitted through the prism at each wavelength. The fluid refractive index $n_{\text{fluid}}(\lambda)$ is then given by

$$n_{\text{fluid}}(\lambda) = \frac{\sin\left[\dfrac{\alpha + \delta(\lambda)}{2}\right]}{\sin\left(\dfrac{\alpha}{2}\right)} n_{\text{gas}}(\lambda),$$

where α is the prism apex angle, $\delta(\lambda)$ is the measured minimum deviation angle, and $n_{\text{gas}}(\lambda)$ is the index of the N_2 ambient ($n_{\text{nitrogen}} = 1.0003$, approximately). The index measurement accuracy is typically $\sim 3 \times 10^{-4}$, even though the method can, in principle, be accurate to ~ 1 to 10 ppm.

When designing high index immersion fluids, it is useful to consider the different contributing factors to the refractive index at the lithographic wavelength. It is also useful to consider the d-line index and the spectral dispersion of the index independently, since these two terms can vary relatively independently with a fluid's physical properties. For example, consider the refractive index of a 17.6-megohm water sample (Fig. 11). The refractive index at 193 nm (n_{193}) is shown along with the d-line index (n_d) and the dispersion Δn, where Δn is defined as $\Delta n \equiv n_{193} - n_d$. From this figure, we see that the 193-nm index of water (1.437) consists of a d-line index of 1.334 and a dispersion of 0.103. These two contributions to the lithographic index are useful materials parameters when comparing different fluids.

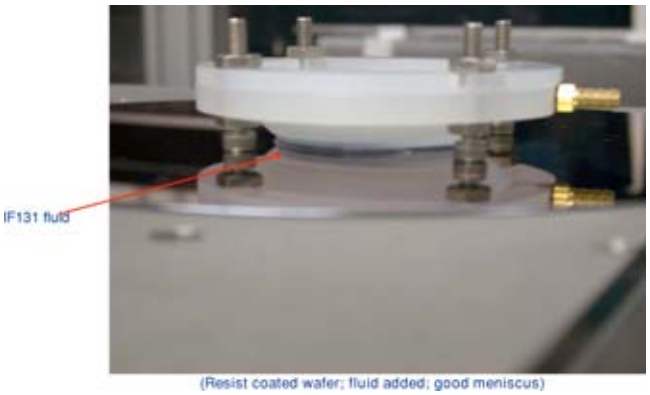

Fig. 10 Showerhead/fluid compatibility test.

3.1.2 *Optical absorbance measurements*

The fluid samples' optical absorbances were determined by measuring the transmission of fluid samples of different thicknesses using a Harrick Scientific Corporation (Ossining, NY) Demountable Liquid Cell model DLC-M13, or a modified long-path length cell that permitted up to 10-cm-long optical paths. Teflon spacers of various thicknesses were used to establish the desired path lengths up to 10 cm. The spacers were sandwiched between two 2-mm-thick, 13-mm or 25-mm-diameter-CaF_2 windows. The optical absorbance per cm (base 10) was then determined by

$$A/\text{cm} = \frac{\log_{10}(T_1) - \log_{10}(T_2)}{t_2 - t_1},$$

where T is the transmission and t is the thickness or path length in the fluid and A/cm is the absorbance per centimeter. If more than two path lengths are measured, using

$$T_n(\lambda) = T_0(\lambda)\exp[-\alpha(\lambda)t_n],$$

one can solve the resulting system of equations and arrive at a standard deviation of the optical absorbance per centimeter reproducibility from the multiple measurements.

For the 17.6-megohm water sample, the measured absorbance is 0.101/cm with a reproducibility standard deviation

Table 3 Optical parameters of different candidate immersion fluids for 193-nm immersion lithography.

Class	Fluid	*n* (193 nm, 22 °C)	Δ*n* (193-d)	Abs/cm (193 nm)	Urbach Edge pos. (nm)	Urbach width (nm)
First generation Fluid	Water	1.437	0.103	0.101	185.2	3.5
Acid	Sulfuric	1.526	0.094			
Acid	Phosphoric	1.537	0.102			
Surfactants	SDS	1.472	0.109			
QA salt	TMA acetate	1.426	0.09			
Silicates	TEOS	1.5	0.114	0.25	184.9	3.2
Linear alkanes	*n*-decane	1.549	0.134	0.19	177.1	2.5
Linear alkanes	*n*-hexadecane	1.581	0.142	0.41	181.9	4.9
Cyclic alkanes	cyclohexane	1.571	0.141	0.09	180.7	2.3
Cyclic alkanes	cyclooctane	1.615	0.152	0.17	183.3	2.9
IF	IF131	1.642	0.166	0.17	190.4	2
IF	IF132	1.644	0.163	0.083	187.1	2.3
IF	IF169	1.656	0.165	0.16	188.3	2.9
IF	IF175	1.664	0.165			

of 0.009/cm (Fig. 12). The 193-nm optical absorbance of high purity water is typically 0.01/cm, but the absorbance varies strongly with the presence of small amounts of absorbing extrinsic impurities, as must be the case here.

3.2 *Analytical Approaches*

With the immersion fluids' two critical properties being refractive index and optical absorbance at the lithographic wavelength, it is useful to have analytical approaches to address the issues that arise in these two properties as a means to understanding and optimizing fluid performance.

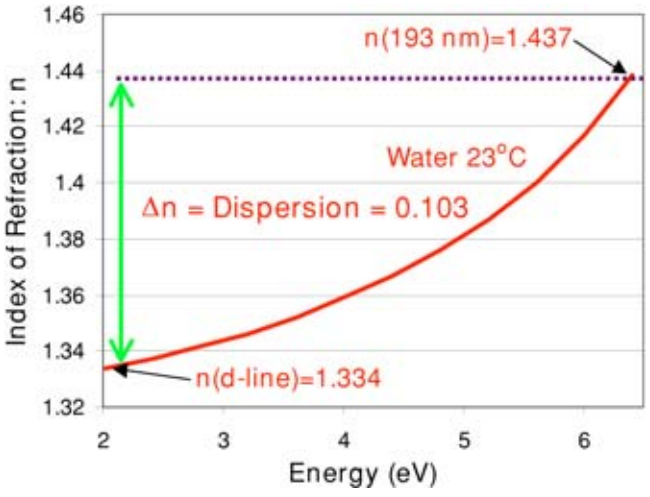

Fig. 11 Spectrum of the refractive index of 17.6-megohm water, showing n_d, Δn, and n_{193}.

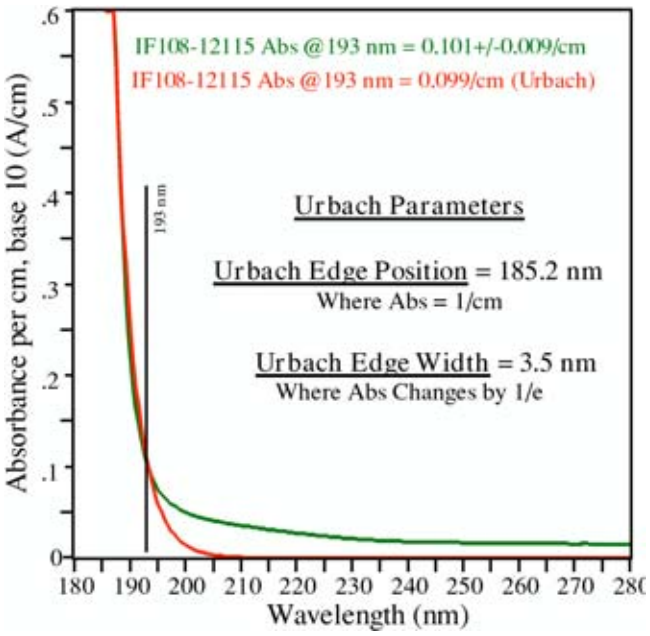

Fig. 12 Optical absorbance of 17.6-megohm water, measured using relative transmission measurement at three thicknesses. The Urbach edge fit to this absorption edge is also shown along with the Urbach fit parameters.

3.2.1 *Lorentz oscillator modeling*

The Lorentz oscillator[9] (LO) is a useful tool for modeling complex optical properties. The optical properties of a Lorentz oscillator model can be solved analytically, and they represent an exact solution to Maxwell's equations of light for the response of a simple harmonic oscillator to an electromagnetic wave. Using the quantum mechanical form of the Lorentz oscillator and allowing the construction of models involving multiple oscillators, one can build models and determine their complex optical property responses. Consider the Lorentz oscillator equation for the complex dielectric function (ε) as a function of photon frequency (ω);

$$\hat{\varepsilon}(\omega) = 1 + \frac{4\pi Ne^2}{m} \sum_j \frac{f_j}{(\omega_j^2 - \omega^2) - i\Gamma_j \omega}.$$

Here Γ_j is the oscillator width, ω_j is the oscillator frequency, N is the electron density, and f_j is the oscillator strength. The plasma frequency ω_p is directly related to the electron density N;

$$\omega_p = \frac{4\pi Ne^2}{m},$$

and in the quantum mechanical Lorentz oscillator model, the oscillator strengths are defined to sum to 1; $\Sigma_j f_j = 1$. When one has the dielectric function of the LO, one can calculate the complex refractive index from the dielectric function as follows: $\varepsilon_1 + i\varepsilon_2 = (n+ik)^2$. One can also calculate the absorption coefficient α from the extinction coefficient: $\alpha = 4\pi k/\lambda$.

We then construct an LO model using three oscillators to represent low-, medium-, and high-energy bonding in the material, and we adjust the plasma frequency and the oscillator energies, widths, and strengths, to yield a model that has the same spectral refractive index as water. Such a model, reproducing water's index, is shown in Fig. 13. This model is not unique, but it is useful to demonstrate the coupled nature of a material's absorption and its refractive index. It allows us to vary the model parameters to see how they affect the values of n_d, n_{193}, and Δn along with the coupled absorption and the absorption edge. For example, it allows us to see how a material's density (represented by the plasma frequency) or the absorption edge energy (represented by the energy and width of the first LO) can be varied. It also shows how an increase in the oscillator strength of the first oscillator (f_1) can increase the dispersion of the refractive index.

3.2.2 *Urbach analysis of absorption edges*

Urbach edge analysis is a useful way to parametrically characterize a fluid's optical absorption edge and to distinguish intrinsic and extrinsic absorbance contributions.[10,11] Urbach[12] originally observed that a material's optical absorption (for energies below the fundamental optical absorption edge) is exponential in nature and can be characterized by

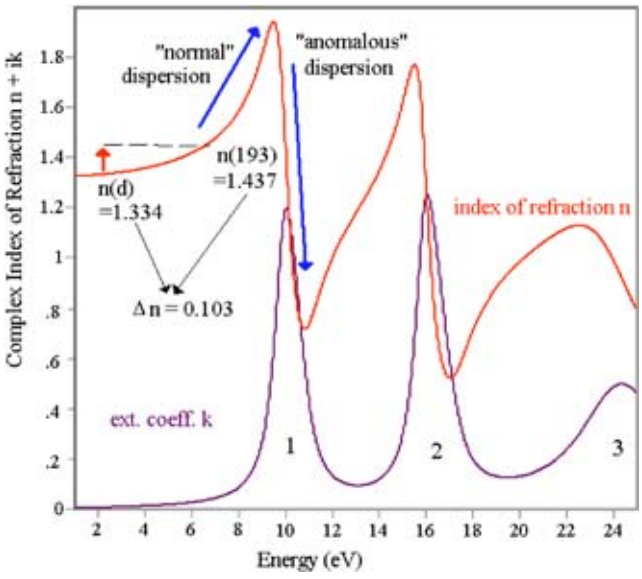

Fig. 13 The refractive index n and extinction coefficient k of a Lorentz oscillator model, using three oscillators, which mimics the index and dispersion of water in the UV.

$$\alpha(E) = \exp\left(-\frac{|E - E_0|}{W}\right),$$

where the absorption coefficient α as a function E is characterized by the Urbach edge energy (E_0) and the Urbach width (W), which is related to the slope of the Urbach edge.

Figure 12 shows the Urbach edge fit to the optical absorption edge of 17.6-megohm water. The Urbach edge fits underneath the measured absorption edge for energies below the fundamental absorption edge, the Urbach edge position is 185.2 nm [using the nm⇔eV conversion λ(nm) =1239.8/E(eV)], and the Urbach width is 3.5 nm. Typically, we find that the standard deviation of the Urbach edge position is ~1.6 nm and of the Urbach edge width is 0.3 nm. There is a correlation of the Urbach edge position with the optical absorbance of the sample and, therefore, Urbach parameters should be compared for samples with comparable absorbances. We can also compare the absorption coefficient at 193 nm for the measured absorbance (0.101/cm) and the Urbach absorption edge (0.099/cm). Pure water's optical absorbance at 193 nm is 0.01/cm, so in this case, the broad, diffuse nature of the extrinsic absorbers does not allow the Urbach edge fit to distinguish the extrinsic contributions from the intrinsic contributions to the optical absorbance.

4 Classes of Second-Generation Immersion Fluids

To meet the Table 1 property requirements, several groups have pursued candidates for second-generation 193-nm immersion fluids. Water additives are one large class being reported in the literature. For example, researchers at Rochester Institute of Technology (RIT)[13] have reported on sulfuric and phosphoric acids as second-generation immersion fluid candidates, while researchers at Columbia[14] have reported on surfactant additives to water. Also, researchers at

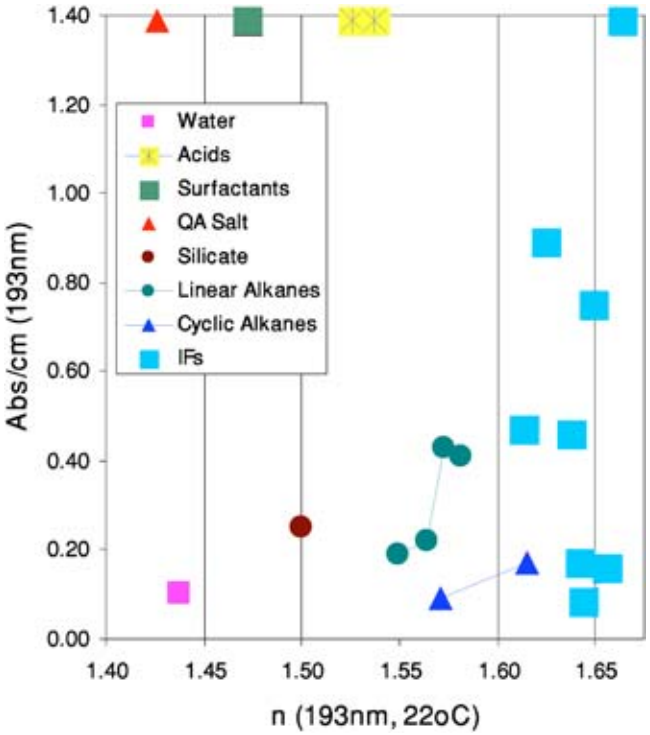

Fig. 14 Refractive index and absorption coefficient of immersion fluid candidates at 193 nm. Fluids with absorbances above 1.4/cm are shown at the top line in the property map. The second-generation property goals are an index of refraction above 1.6 and an absorbance below 0.2/cm.

Clemson[15] have presented nanoparticle additives to water, and researchers at the University of Texas, Austin[16] have reported on quaternary ammonium salts as water additives. In addition, researchers at Air Products[17] and JSR[18] have also presented results on second-generation fluids.

We consider the high index fluid candidates in three groups: aqueous, organic, and (in Sec. 5) the immersion fluids we have been developing. When considering immersion-fluid groups, it is useful to develop an optical property map that shows the lithographic index and the optical absorbance at 193 nm. Figure 14 shows the index/absorbance map for various fluids, the initial standard being the first-generation fluid, water. We previously did similar studies to survey candidate fluids for 157-nm immersion lithography.[19]

4.1 *Aqueous Candidates*

As previously noted, RIT has presented work on acids such as concentrated sulfuric and phosphoric acids. The indices we measure are in the range of 1.5 to 1.55. Other groups are looking at surfactants (Columbia) and quaternary ammonium salts (University of Texas, Austin). In our measurements, these classes have indices of less than 1.5 at 193 nm.

4.1.1 *Optics of mixtures*

In the case of aqueous blends of acids, salts, or surfactants, it is useful to consider the possible impact of mixtures on the refractive index at 193 nm using a Lorentz oscillator model to simulate the mixture. Figure 15 shows two 3-LO

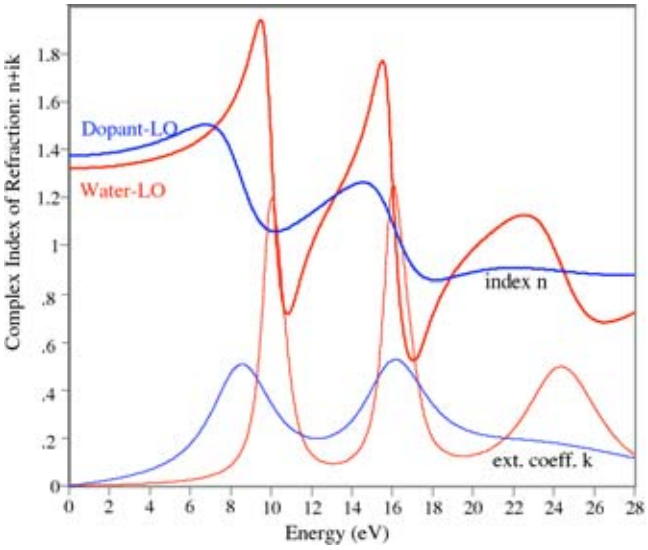

Fig. 15 Lorentz oscillator models that mimic the index dispersion from d line to 193 nm for water and TEOS.

models: one mimics the index and dispersion in the visible and UV range of water; the other mimics the index and dispersion of tetraethylorthosilicate (TEOS) (see Sec. 4.2). The difference between the models is in the energy and broadening of the oscillators, and these changes lead to differences in the complex refractive index. Using these LO models and adding the oscillators in different ways, we can develop two models that represent different possible mixture types of the dopant in water. We assume a 50:50 ratio of water to dopant.

Figure 16 shows the spectral refractive index for the water and the dopant LO model and also shows the data for

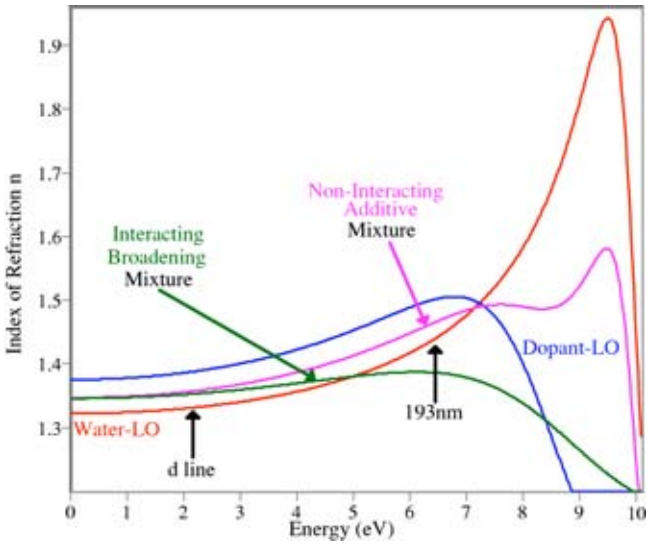

Fig. 16 Lorentz oscillator models, representing 50:50 mixtures of water and a TEOS-like dopant, based on two approaches: a noninteracting (additive) mixture and an interacting (broadening) mixture. Note the changes in the n_d and n_{193}, and the dispersion for the two different models.

two cases: first, a noninteracting mixture; and second, a mixture in which there is an interaction between the water and the dopant.

In the noninteracting mixture, we simply sum the oscillators of the water and dopant materials, while reducing the oscillator strength of each oscillator to represent its 50% contribution to the new mixture. This noninteracting "additive" mixture represents a case in which the water and dopant species do not modify each other's properties, and the 50:50 mixture shows a refractive index that is halfway between the two components. In this case, the dopant's higher refractive index is reduced in direct proportion to the concentration of the lower-index component, water.

Although this gives rise to simple rule-of-mixture behavior, the case of a noninteracting mixture may well represent a special, and even unusual, case. The more general case is one in which the dopant shows some interaction with water and each undergoes some modification, be it simple complexation or a more fundamental chemical reaction. Here, we expect that the different LOs in the resulting mixture are modified from the component materials by interaction. To represent this case, we take the six oscillators present in the two LO models for water and dopant, and produce a mixture model that consists of three oscillators having energies between those of water and dopant, and widths that are determined by the sum of the component materials' widths and the energy difference between the component oscillators. We call this an interacting broadening mixture model, since the interactions between the two components lead to a broadening of the oscillators in the mixture. In this case, we see a radical change in the model's refractive index: the behavior no longer follows the rule of mixtures, but instead shows a reduced d-line index and a refractive index that is less than water's at 193 nm. So, unlike the rule of mixtures (under which we obtain a refractive index that is between that of the two components), in the interacting broadening model, the index of the mixture is actually less than the indices of either component at 193 nm. This results because, although the broadening does not change n_d dramatically, it does significantly reduce the dispersion from 0.107 for the noninteracting model to 0.034 for the interacting model.

LO modeling thus suggests that mixtures may show counterintuitive changes in refractive index when the components of the mixture interact chemically or physically. This is because the refractive index consists of n_d and the dispersion, and the magnitude of the dispersion varies with the width and broadening of the absorption features. The close relationship between absorption and index (as defined by the Kramers-Kronig relations[20–22]) suggests that a more complete analysis is required. Indeed, simple LO models, which maintain Kramers-Kronig consistency in absorption and index, may usefully predict optical performance in real systems.

4.2 *Organic Candidates*

Beyond the materials classes already referred to, the optical properties of hydrocarbons such as alkanes merit consideration. In Fig. 14, the index of refraction for four linear and cyclic alkanes is shown, and these fluids have indices of more than 1.55. An organosilane, tetraethylorthosilicate (TEOS), has an index of refraction on the order of 1.5, and therefore does not achieve the $n_{193}=1.6$ criteria for a second-generation fluid.

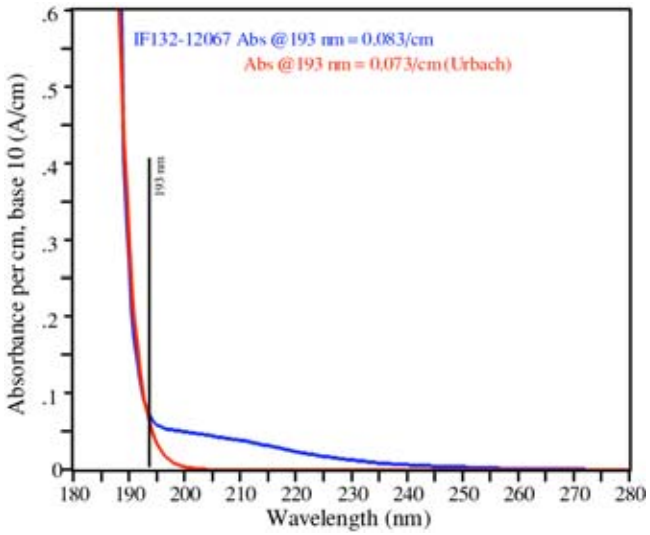

Fig. 17 Optical absorption edge and Urbach edge for IF132 showing a low absorbance second-generation immersion fluid.

4.3 *High-Index, 193-nm, Second-Generation Immersion Fluids*

We have developed second-generation candidate fluids that exceed the refractive index requirement and some that also meet the optical absorbance requirement.

4.3.1 *Low-absorbance fluids*

Figure 17 shows the optical absorption edge of IF132 along with an Urbach edge fit. This fluid has an absorbance of 0.083/cm. Its Urbach edge position is 187.1 nm, whereas water is 185.2 nm, and the Urbach width is 2.3 nm, while the Urbach width of water as shown in Fig. 17 is 3.5 nm.

4.3.2 *High-index fluids*

Figure 18 shows a comparison of water's spectral refractive index with that of a second generation candidate, IF175. IF175 has a d-line index of 1.499, and water has an index of 1.33. The dispersion of IF175 is 0.165, which is much larger than the dispersion of 0.103 for water. From this, the refractive index of IF175 at 193 nm is 1.664, a substantial improvement on water's index of 1.437.

5 Resist and Topcoat Testing with Second-Generation Immersion Fluids

Imaging tests on an interferometric immersion test rig with DuPont's IF131 and IF132 immersion fluids indicate very good compatibility with current resists and topcoats. The refractive index of 1.65 and absorbance value of 0.08/cm is useful in the context of technology development for the 32-nm node on an interferometric test rig.

Initial tests were run with showerheads, and fluid wetting characteristics on resist and topcoat were studied (Fig. 10). Measurements of fluid contact angles were made; Table 2 compares contact angles with water for a range of materials.

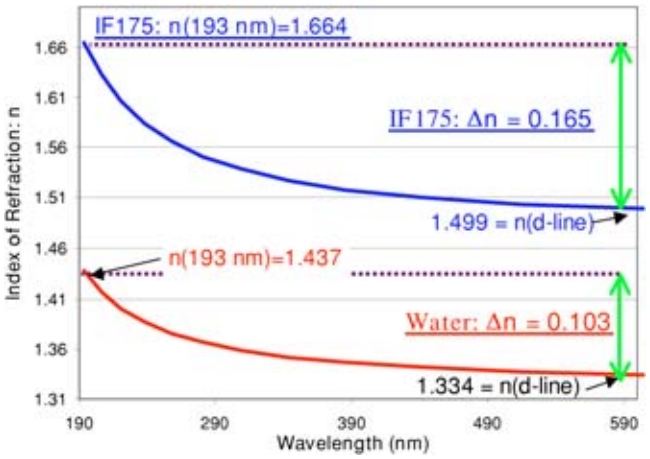

Fig. 18 Spectral refractive index of IF175 compared to the refractive index of water. Note IF175's increased n_d, dispersion Δn, and n_{193}.

Topcoats are now used in development laboratories to isolate resists from the effects of the immersion fluid and from airborne, amine-type contamination. Many companies have supplied the topcoats and resists for imaging tests with the new immersion fluids. Table 4 lists some of the resists and topcoats tested along with details of the processing settings used. Hot-plate times and temperatures are specified for resist post-apply (PAB) and post-exposure (PEB) bakes. Coating thicknesses are also specified. Wafers were exposed on the test rig and developed using a standard aqueous 0.26 normal tetra methyl ammonium hydroxide TMAH solution. The topcoat was removed using the standard develop process.

Initial tests with topcoats indicated a problem: topcoats such as TOK TSP-3A had a refractive index that was too low for 32-nm work; 32-nm testing using the topcoats with the highest reported refractive indices has been done. Resist systems generally have refractive indices of approximately 1.7; this allows 32-nm printing.

We tested a number of resist samples with topcoats, and the initial results are shown in Figs. 19 and 20. These results were obtained with photoresist film thicknesses of 63 nm on bottom antireflection coating (BARC) (typically ARC29, 85 nm thick) and with an immersion fluid thickness of 4 mm. The two DuPont fluids, IF131 and IF132, were successfully used to print 32-nm L/S using TE mode illumination at a 193-nm wavelength. The results were good: the two fluids showed similar resist profiles, and there was no deterioration or observable fluid effect on either the topcoats or the resists. The Sumitomo resist PAR-817 was used, and we estimate from these figures a line edge roughness (LER) of 3 nm, but more accurate LER measurements will be done in the future.

Further tests were conducted with a variety of different topcoats and a different resist (Fig. 21). We saw differences

Table 4 Resists and topcoat tested.

Supplier	Resist	Thickness (nm)	PAB	PEB
JSR	AR1941J	70	115C/90 s	115C/90 s
Sumitomo	PAR 817	70	130C/60 s	110C/60 s
Sumitomo	AJ4385S45	70	110C/60 s	115C/60 s
Fuji Arch	HI1010-03	70	115C/60 s	130C/90 s
Rohm & Haas	XP1020A	70	120C/90 s	120C/90 s

Supplier	Top Coat	Thickness (nm)	Refractive index at 193 nm
TOK	TILC019	130	1.4759
TOK	TILC016	70	1.6651
JSR	TCX007	130	1.53
TOK	TSP-3A	38	1.43
Central Glass	AC-1	38	1.502
Central Glass	AC-2	30	1.502
Central Glass	AC-12	30	1.591
Central Glass	AC-13	30	1.614
Central Glass	AC-14	30	1.618

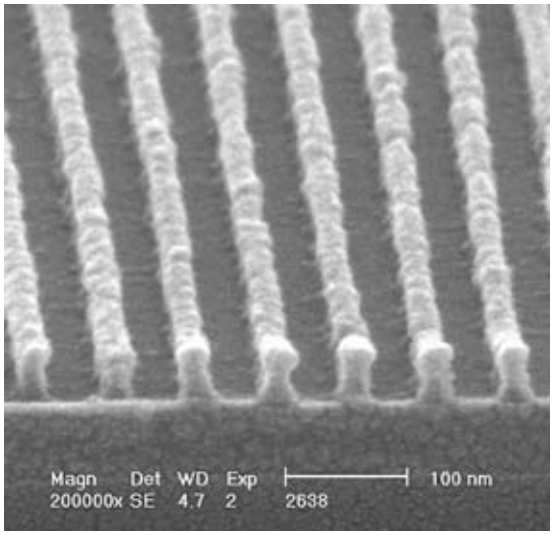

Fig. 19 Immersion interference imaging showing 32-nm 1:1 line/spaces using IF131.

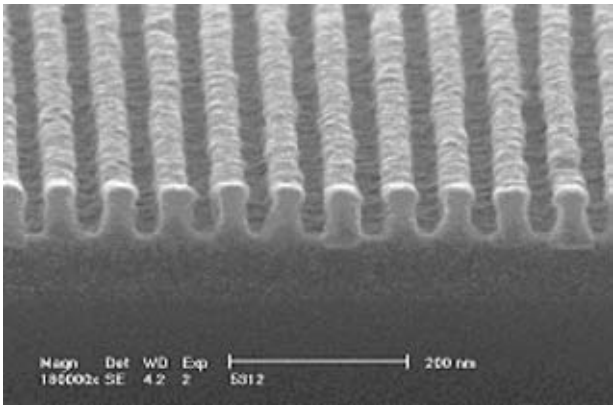

Fig. 20 Immersion interference imaging showing 32-nm 1:1 line/spaces using IF132.

in fluid wetting effects with different topcoats. It became clear that certain topcoats interact with the resist, and resist profile height is lost in development. This may be an intermixing effect.

Further tests of a matrix of topcoats and resists are now being done. We are assessing image quality, fluid contact angles, and wetting. Line-edge roughness, though present, has been better than expected for a chemically amplified resist. This kind of test allows the continued optimization of the resist, both in formulation and in processing parameters.

6 Conclusions

We have developed a number of second-generation high-refractive index fluids for immersion lithography at 193 nm. These highly transparent fluids have 193-nm indices of up to 1.67. To understand the behavior and performance of the different fluid classes, we use spectral index measurements to characterize the index dispersion, with Urbach optical absorption edge analysis, and LO modeling. The DuPont fluids with refractive indices of 1.65 and absorption at 193-nm wavelength $<0.1/\mathrm{cm}$ will allow 38-nm node imaging, potentially in production. These fluids allow 32-nm node technology development.

We demonstrate 32-nm 1:1 line/space imaging using two second-generation candidate fluids. This represents a major advance in optical lithography and immersion fluid development.

For production viability at 32 nm, a number of improvements are required in fluid, topcoat, and resist. The refractive indices for resist and immersion fluid must be pushed up toward 1.9 to allow 32-nm lithography to be conducted at k factors of approximately 0.30. The application of the methods used to produce and identify the second-generation immersion fluids is likely to yield refractive index increases in both resist and topcoat systems.

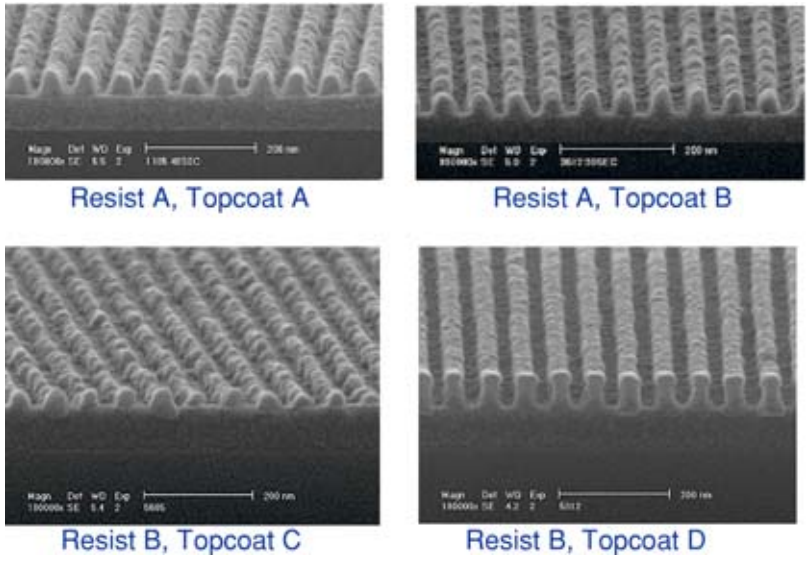

Fig. 21 32-nm imagery using ASML interference immersion test rig with DuPont IF-132 immersion fluid for a matrix of resists and topcoats.

If process window size becomes an issue for 45-nm node imaging, the availability of new, high-index immersion fluids may mean an early replacement of water as the immersion fluid.

Lens costs must be addressed; they are related to the size of the optics, and hence, the numerical aperture. This is likely to become the major issue with ArF immersion for the 32-nm node. This issue may drive smaller field sizes and an 8× stepper reduction ratio for the 32-nm node.

Acknowledgments

The authors acknowledge the assistance of John Schmieg and Michael Mocella of DuPont. Simulation work support by Eric Hendrix, Jan Hermans, and Lieve Van Look of IMEC is appreciated. Acknowledgment to ASML-Wilton staff: Mark Riggs, Selina Islam for SEM support; Ron Albright, Christine Dadarria, Chistopher Chmielewski, and Bob McInnes for wafer and data measurement support; and Aleksandr Khmelichek for fluid showerhead work. Support from ASML-Veldhoven by Jan Mulkens and Jos Benschop is also significant. Twinscan data were supplied by the ASML-Veldhoven demonstration laboratory and wafer processing group. Also thanked are Sumitomo, OHKA, Fuji/Arch, Rohm and Haas, Central Glass, Air Products, and JSR for their support and samples for 32-nm imaging.

References

1. The International Technology Roadmap for Semiconductors (ITRS) is available at http://www.itrs.net/Common/2004Update/2004Update.htm.
2. M. Totzeck, P. Graupner, T. Heil, et al., "How to describe polarization influence on imaging," *Proc. SPIE* **5754**, 23–37 (2005).
3. D. G. Flagello, S. G. Hansen, B. Geh, et al., "Challenges with hyper-NA (NA>1.0) polarized light lithography for sub−lambda/4 resolution," *Proc. SPIE* **5754**, 53–68 (2005).
4. S. Teuber, K. Bubke, et al., "Determination of mask-induced polarization effects occurring in hyper-NA immersion lithography," *Proc. SPIE* **5457**, 543–554 (2005).
5. C.,Chen, T. Gau, L. Shiu, and B. Lin, "Mask polarization effect in hyper-NA systems," *Proc. SPIE* **5754**, 1128–1137 (2005).
6. J. H. Burnett, S. G. Kaplan, et al., "High-index materials for 193-nm and 157-nm immersion lithography," *Proc. SPIE* **5754**, 611–621 (2005).
7. R. H. French, M. K. Yang, M. F. Lemon, et al., "Immersion fluid refractive indices using prism minimum deviation techniques," *Proc. SPIE* **5377**, 1689–1694 (2004).
8. R. A. Synowicki, G. K. Pribil, G. Cooney, C. M. Herzinger, S. E. Green, R. H. French, M. K. Yang, J. H. Burnett, and S. Kaplan, "Fluid refractive index measurements using roughened surface and prism minimum deviation techniques," *J. Vac. Sci. Technol. B* **22**(6), 3450–3453 (2004).
9. F. Wooten, *Optical Properties of Solids*, Academic Press, New York (1972).
10. M. E. Innocenzi, R. T. Swimm, M. Bass, R. H. French, A. B. Villaverde, and M. R. Kokta, "Room temperature optical absorption in undoped α-Al_2O_3," *J. Appl. Phys.* **67**(12), 7542–7546 (1990).
11. M. E. Innocenzi, R. T. Swimm, M. Bass, R. H. French, and M. R. Kokta, "Optical absorption in undoped yttrium aluminum garnet," *J. Appl. Phys.* **68**(3), 1200–1204 (1990).
12. F. Urbach, "The long-wavelength edge of photographic sensitivity and of the electronic absorption of solids," *Phys. Rev.* **92**, 1324 (1953).
13. J. Zhou, Y. Fan, A. Bourov, F. Cropanese, A Estroff, and B. W. Smith, "Immersion fluids for high NA 193nm lithography," *Proc. SPIE* **5754**, 630–637 (2005).
14. K. Lee et al., "Amplification of the index of refraction of aqueous immersion fluids by ionic surfactants," *Proc. SPIE* **5753**, 537–553 (2005).
15. W. E. Conley, P. Zimmerman, G. Chumanov, D. D. Evanoff, I. Luzinov, and K. Klep, "High refractive index nanocomposite liquid for 193nm immersion lithography," *Proc. SPIE* **5753** (2005).
16. J. C. Taylor, R. Shayib, et al., "Fluids and resists for hyper NA immersion lithography," *Proc. SPIE* **5753**, 836–846 (2005).
17. P. Zhang, B. Budhlall, et al., "High refractive index immersion fluids for 193nm immersion lithography," *Proc. SPIE* **5754**, 622–629 (2005).
18. T. Miyamatsu, Y. Wang, et al., "Material design for immersion lithography with high refractive index fluids," *Proc. SPIE* **5753**, 10–19 (2005).
19. R. R. Kunz., M. Switkes, R. Sinta, J. E. Curtin, R. H. French, R. C. Wheland, C. C. Kao, M. P. Mawn, L. Lin, P. Wetmore, V. Krukonis, and K. Willams, "Transparent fluids for 157nm immersion lithography," *J. Microlithogr., Microfabr., Microsyst.* **3**(1), 73-83 (2004).
20. M. L. Bortz and R. H. French, "Quantitative, FFT-based, Kramers Kronig analysis for reflectance data," *Appl. Spectrosc.* **43**(8), 1498–1501 (1989).
21. R. H. French, D. J. Jones, H. Müllejans, S. Loughin, A. D. Dorneich, and P. F. Carcia, "Optical properties of aluminum nitride: determined from vacuum ultraviolet spectroscopy and spectroscopic ellipsometry," *J. Mater. Res.* **14**, 4337–4344 (1999).
22. G. L. Tan, L. K. DeNoyer, R. H. French, M. J. Guittet, and M. Gautier-Soyer, "Kramers Kronig transform for the surface energy loss function," *J. Electron Spectrosc. Relat. Phenom.* **142**, 97–103 (2004).

Roger H. French holds a PhD in materials science from MIT where his work involved vacuum ultraviolet spectroscopy on Al_2O_3 from 80 to 800 nm. He is a senior research associate in materials science in Central Research at the DuPont Company in Wilmington, Delaware, and also an adjunct professor of materials science at the University of Pennsylvania. His research is in optical properties and electronic structure of ceramics, optical materials, and polymers. His work on lithography materials has produced attenuating phase shift photomasks, pellicles, and photoresists, and now is focused on materials for immersion lithography. In addition he works in near-field optics of particulate dispersions and London dispersion forces and electronic structure of surfaces and interfaces. His work has produced 10 patents and 115 published papers.

Harry Sewell is a Director of Technology at ASML-Wilton, Connecticut. He received a BSc (physics) with honors and PhD (electrical engineering, materials science) from Imperial College of Science and Technology, London University, 1972. His research was on slow states in thin film transistors. He joined Philips Research Laboratories, Redhill, United Kingdom, and worked on thin film technology and e-beam lithography. He immigrated to Canada in 1979 to join Bell Northern Research and worked on NMOS and CMOS process design. He joined Perkin Elmer in 1982 to work in optical lithography. He worked on the development of scanning and step and scan systems for I-line, deep-uv, and 157-nm wavelengths. He has written many papers and given many presentations on the subject of lithography. He is currently working on immersion, imprint, and advanced lithographic techniques at ASML-Wilton.

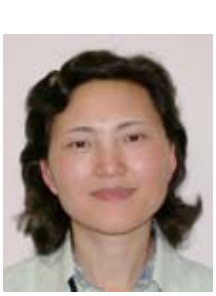

Min K. Yang is a staff technologist at DuPont. She received her master's degree in materials science and engineering from Virginia Tech in 1994. She joined DuPont in 2000 and has been involved in several projects. Currently she works on immersion lithography, where she focuses on optical properties testing of immersion fluid. She has contributed to several papers and patents in the area of immersion lithography.

Sheng Peng received her PhD degree in organic chemistry from the Shanghai Institute of Organic Chemistry (SIOC, Chinese Academy of Sciences) in the year 2000, followed by postdoctoral research in organic synthesis and biochemistry at the University of Illinois at Urbana-Champaign. In 2003, she joined DuPont Central Research and Development. Since then she has been working on material for 157- and 193-nm immersion lithography, focusing on high refractive index and low absorbance 193-nm immersion fluids.

Diane McCafferty is a system design engineer at ASML-Wilton. She holds an MS in chemical engineering from the University of Virginia and has more than 20 years experience in the semiconductor industry working at IBM, SVGL, and now ASML. Currently, she is a project lead engineer on the research of high-*n* immersion fluids at ASML.

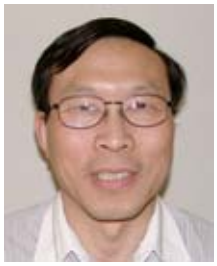

Weiming Qiu received his PhD degree in chemistry from Shanghai Institute of Organic Chemistry, China, in 1987. After postdoctoral research with D. J. Burton at the University of Iowa, he joined DuPont's Central Research and Development Department in 1995. His research interests are organofluorine chemistry and fluoropolymer chemistry. Recently, he has been involved in the development of pellicle, resist, and immersion fluids for 157 -and 193-nm lithography. He has contributed to more than 40 research papers, book chapters, and review articles. He is an inventor or coinventor for eight patents.

Robert C. Wheland received a PhD in organic chemistry from Harvard University in 1971. After a year of postdoctoral research at the Calfornia Institute of Technology, he joined DuPont as a research chemist. His principal research areas at DuPont have been in the areas of nylon amidation catalysis, free radical initiator chemistry, and fluoropolymers.

Michael F. Lemon is a research technician at the DuPont Experimental Station. He received his associates degree in environmental engineering from Delaware Technical and Community College in 1980. He joined DuPont in 1984 and since then has worked in the material science group of the Central Research Division. His current research is in materials for immersion lithography focused on radiation durability, lithographic printing, and fluid handling systems for 193-nm immersion lithography. He has contributed to papers and patents in the area of immersion lithography and lithography materials during the last ten years.

Louis Markoya is a principal engineer working on the design and development of immersion lithography systems. He has more than 20 years experience in the semiconductor industry working at ITT, Intel, SVGL, and ASML.

Michael K. Crawford received his PhD in physical chemistry from Columbia University in 1981. After postdoctoral study in the physics department of the University of California, Berkeley, he joined the Central Research and Development Department at DuPont in 1985, where he is currently a senior research associate in Central Research and Development. At DuPont, his areas of research have included high-temperature superconductivity; synchrotron x-ray and neutron scattering studies of structural phase transitions and magnetism in transition metal oxides; infrared, Raman, and optical spectroscopy of hydrofluorocarbons and photoresists; and luminescence spectroscopy of inorganic and organic phosphors.